INORGANIC CHEMISTRY FRONTIERS

RESEARCH ARTICLE

View Article Online
View Journal | View Issue

Check for updates

Cite this: *Inorg. Chem. Front.*, 2024, **11**, 2049

X-ray-activated ultra-long UVA persistent luminescence from a Bi-doped perovskite $LaGaO_3$ for photodynamic activation†

Bo-Mei Liu, [a,b] Yue Lin,[a] Yingchun Liu,[a] Shanqing Zhang,[b,a] Jing Wang, *[c] Hui Zhang*[a,d] and Jesse Zhu [b,a]

Ultraviolet (UV) emitting persistent luminescence (PersL) materials have aroused significant interest, owing to their unique self-illuminating high-photo-energy feature under excitation-free conditions. In particular, the advent of X-rays as a charging source for UV PersL has facilitated the control of PersL properties and triggered a breakthrough in possible applications such as X-ray imaging techniques, phototherapy, photocatalysis, and optical information storage. Here, we present novel PersL materials that exhibit ultra-long UV emission for over 2000 h, as detected with a spectrometer. Experimental characterization revealed that the intrinsic oxygen vacancies associated with the local structure of the perovskite $LaGaO_3$ can function as traps, which have super capabilities in energy collection and storage triggered by X-ray irradiation. Notably, this design concept is guided by utilizing an oxygen-defect perovskite as a host, which can serve as powerful guidance for expediting the discovery of new PersL materials. Moreover, due to excellent UV PersL performances, the proposed photodynamic therapy (PDT) platform $LaGaO_3$:Bi,Sb@g-C_3N_4 demonstrates excellent PDT efficiency *in vivo* using low-dose X-ray irradiation. Our discovery of this UV PersL material is expected to provide directional solutions and novel perspectives for the development and application of UV luminescence technology.

Received 17th December 2023,
Accepted 19th February 2024

DOI: 10.1039/d3qi02604c

rsc.li/frontiers-inorganic

Published on 21 Kudo 2024. Downloaded on 09/10/2024 2:28:35 PM.

1. Introduction

PersL with a long-lived emission lifetime is a unique optical phenomenon that has received considerable attention in the fields of displays and lighting, biomedicine, advanced sensors, and energy.[1–4] Unfortunately, only a handful of persistent phosphors have been commercialized owing to their unusual properties since the discovery of the bright green PersL of $SrAl_2O_4$:Eu^{2+},Dy^{3+} in 1996 by Matsuzawa *et al.*[5] Currently, visible PersL materials are rapidly developing and achieving commercial success for diverse applications. Representative examples include Y_2O_2S:Eu^{3+},Mg^{2+},Ti^{4+} (red, >5 h), $SrAl_2O_4$:Eu^{2+},Dy^{3+} (green, >30 h), and $CaAl_2O_4$:Eu^{2+},Nd^{3+} (blue, >10 h).[6,7] Recently, PersL in the near-infrared region (NIR, 650–1700 nm) has gained attention for promising bioimaging applications, driven by the discovery of $La_3Ga_5GeO_{14}$:Cr^{3+} (NIR, >8 h).[8] Exploring materials like $Zn_3Ga_2Ge_2O_{10}$:Cr^{3+} (NIR, >360 h) and $ZnGa_2O_4$:Cr^{3+} (NIR, >48 h) has opened a new research frontier in PersL materials.[9,10] In stark contrast to the evolving progress in the visible and NIR PersL, research in the UV region (200–400 nm) remains relatively sluggish. There is an increasing trend in the research of UV PersL materials, such as rare-earth-doped phosphors $Lu_2GdAl_2Ga_3O_{12}$:Pr^{3+} and YPO_4:Tm^{3+}.[11–13] Recently, a Pr^{3+}-doped fluoride-based ultraviolet C (UVC, 200–280 nm) PersL phosphor (Cs_2NaYF_6:Pr^{3+}) with a PersL duration of ~2 h after X-ray radiation was achieved.[14] Soon afterward, the $LiYGeO_4$:Bi^{3+} phosphor with intense PersL in the ultraviolet A region (UVA, 315–400 nm) was successfully developed, which exhibits UVA PersL peaking at 350 nm for more than 300 h.[15] However, the lack of excellent UV PersL materials, which can be comparable to classical visible or NIR PersL materials, is hindering the practical application of UV technology.

To date, the world has witnessed the application potential of UV technology in various fields, such as imaging, information encryption, photocatalytic activity, and light-mediated theranostics.[16–18] Photodynamic therapy (PDT), for instance, an emerging cancer treatment solution, has attracted much

[a]*School of Chemical Engineering and Light Industry, Guangdong University of Technology, Guangzhou 510006, China. E-mail: hzhang-gg@gdut.edu.cn*
[b]*Guangdong Laboratory of Chemistry and Fine Chemical Industry Jieyang Center, Jieyang 515200, China*
[c]*School of Chemistry, Sun Yat-sen University, Guangzhou 510006, China. E-mail: ceswj@mail.sysu.edu.cn*
[d]*Wesdon River Powder Paint Scientific Research Co., Ltd, Foshan 528200, China*
† Electronic supplementary information (ESI) available. See DOI: https://doi.org/10.1039/d3qi02604c

This journal is © the Partner Organisations 2024

Published on 21 Kudo 2024. Downloaded on 09/10/2024 2:28:35 PM.

attention from fundamental research to clinics. However, the excitation light utilized in PDT struggles to penetrate tissues, posing a challenge to its further advancement. To overcome this, X-rays have been introduced to transmit energy into depths.[19,20] Regrettably, this technology is plagued by the risks of ionizing radiation injury and tissue ablation induced by prolonged irradiation. Revealingly, by harnessing the capabilities of X-ray-activated visible-NIR PersL materials, which store X-ray energy and act as internal light sources for extended periods of time, the need for repeated excitation is eliminated.[21] This innovation significantly reduces X-ray dosage and duration, enhancing safety and effectiveness. Consequently, substantial progress has been made in biological applications, including long-term photodynamic therapy (PDT), biosensing, and rechargeable bioimaging.[22] Inspired by the above developments and considering the potential applications of UV light, exploring X-ray-activated UV PersL as an alternative luminescent source could be significant. In particular, the UV-blue light is a more efficient (for lots of photosensitizers, *e.g.* g-C_3N_4) PDT activator than visible-NIR light.[23] For widespread applications, UV PersL materials should be excitable and chargeable by deep penetration, less harmful light sources like low-dose (<5 Gy) X-ray light and exhibit a much longer persistence time (*e.g.* >100 h), thus offering an attractive prospect for biomedicine, such as generating energy for long-term light-mediated therapeutics.

Rational syntheses of PersL systems remain elusive, and the design and synthesis of PersL materials primarily rely on empirical approaches. Here, a strategy to prepare new X-ray-activated PersL materials is demonstrated by selecting a defect-containing perovskite (*i.e.* $LaGaO_3$, $LaAlO_3$) as a matrix and utilizing the Bi^{3+} ion as the emitter. The $LaGaO_3$ host, which is famous as an oxygen ionic conductor host material, has shown strong NIR PersL with Cr^{3+} doped under X-ray excitation. It is confirmed that oxygen vacancies (Vo) as trap centers with suitable trap depths can capture carriers and then effectively generate NIR PersL.[24] Moreover, a similar phenomenon of NIR PersL is also found in $LaAlO_3$:Cr^{3+}.[25] Analogously, the potential generality of this strategy is demonstrated with Bi-doped $LaGaO_3$ and $LaAlO_3$ PersL phosphors by utilizing intrinsic Vo to store excitation energy and gradually release it to the emitters.

A proof-of-concept for repeatable and depth-independent photodynamic therapy (PDT) is reported here, utilizing low-dose X-ray-activated UVA PersL materials as an excitation source. The PersL performances (intensity and duration) are the key points to effective PDT treatment and reducing irradiation damage to normal tissues. By taking advantage of X-ray-activated ultra-long UVA PersL in $LaGaO_3$:Bi,Sb, and then coupling it with a photosensitizer, the X-ray-activated $LaGaO_3$:Bi,Sb@g-C_3N_4 PDT platform was fabricated. Indeed, the depth barrier for tissue penetration and efficacy can be broken based on the use of the ultra-long X-ray-activated UVA PersL $LaGaO_3$:Bi,Sb. These properties suggest that the X-ray-activated ultra-long UVA PersL $LaGaO_3$:Bi,Sb is a promising material in clinical settings.

2. Results and discussion

2.1 Structure and luminescence properties of the perovskite $LaGaO_3$:Bi

Perovskite $LaGaO_3$ was chosen as the host, and Bi ions were selected as emitters based on the following concepts: (1) both La and Bi elements possess strong X-ray absorption capabilities, enabling the system to be charged through X-ray excitation; (2) $LaGaO_3$ features a large bandgap and a tendency to form Vo defects that can potentially act as trap centers; and (3) the $^3P_1 \rightarrow {}^1S_0$ transition of Bi^{3+} ions results in UV emission. To validate the scheme, a series of Bi-doped $LaGaO_3$ materials were synthesized *via* the solid-state route. Phase-pure $LaGaO_3$ (JCPDS No. 24-1102) with the perovskite structure was produced before and after the Bi^{3+} ions doping (Fig. 1). In the $LaGaO_3$ crystal structure, there is one 12-coordinate La^{3+} site, one 6-coordinate Ga^{3+} site, and two kinds of coordinated O^{2-} sites. Thus, the ionic radii and valence state results suggest that Bi^{3+} (r = 1.38 Å) occupies the La^{3+} (r = 1.36 Å) sites in the $LaGaO_3$ lattice.

The photoluminescence (PL) and photoluminescence excitation (PLE) spectra of the synthesized $LaGaO_3$:xBi are depicted in Fig. 2a. Under 306 nm excitation, $LaGaO_3$:Bi^{3+} shows emission at 372 nm with the full width at half maximum of 41 nm. By adjusting the concentration of Bi, the optimal chemical composition with x = 0.1% was obtained. Generally, the Bi^{3+} UV luminescence is constituted by the forbidden $^3P_0 \rightarrow {}^1S_0$ and the allowed $^3P_1 \rightarrow {}^1S_0$ optical transitions at room temperature. The long-wavelength excitation band is located at 306 nm ($^1S_0 \rightarrow {}^3P_1$).[26] The maximum of the short-wavelength excitation band ($^1S_0 \rightarrow {}^1P_1$) was outside the detection limit of the spectrometer. For comparison, Fig. 2b confirms that steady-state emission spectral characteristics are identical under both UV light and X-ray excitation. This result indicates that Bi^{3+} ions serve as emitters for both X-ray and UV excitation. When the energy generated in multiple X-ray collisions aligns with the $^1S_0 \rightarrow {}^3P_1$ transition of Bi^{3+}, it initiates the transition of Bi^{3+} from the ground state to the excited state, resulting in emission patterns similar to those observed with UV excitation.

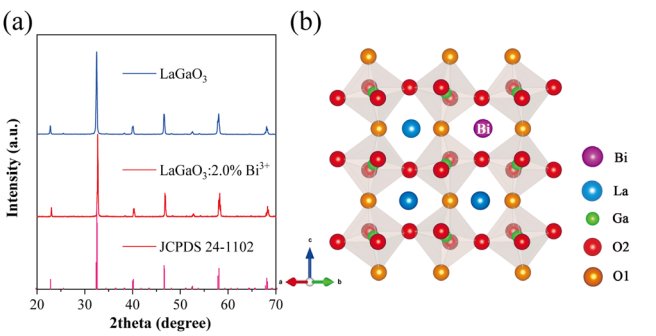

Fig. 1 (a) XRD patterns of undoped and typical Bi-doped $LaGaO_3$. (b) The structure of Bi-doped $LaGaO_3$.

This journal is © the Partner Organisations 2024

Published on 21 Kudo 2024. Downloaded on 09/10/2024 2:28:35 PM.

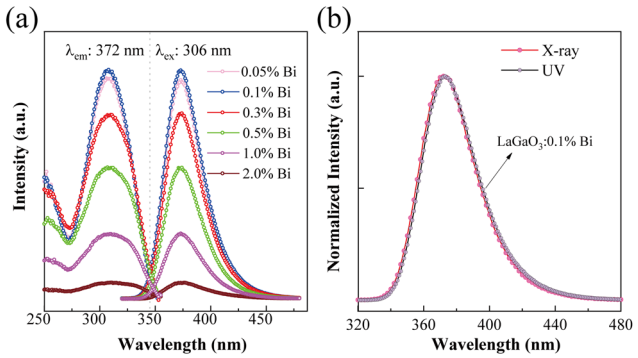

Fig. 2 (a) PL and PLE spectra of $LaGaO_3$:*x*Bi (*x* = 0.05–2%) at room temperature. (b) Normalized emission spectra of $LaGaO_3$:0.1%Bi under irradiation with an X-ray and a 306 nm UV light, respectively.

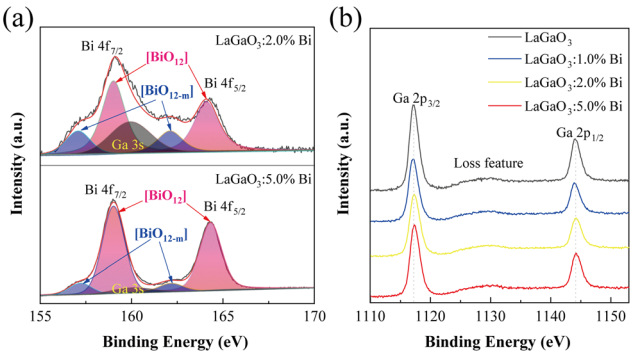

Fig. 4 (a) XPS of Bi 4f and peak deconvolution of 2%Bi and 5%Bi doped $LaGaO_3$. (b) XPS spectra of Ga 2p for typical Bi-doped $LaGaO_3$. Note: Bi 4f photoelectron transitions overlap with the Ga 3s peaks (set at 160 eV),[27] and the peak position and intensity remain unchanged with the change in the Bi ion concentration and do not affect the peak fitting process.

Interestingly, the sample exhibited a strong UV PersL at 372 nm after X-ray irradiation (Fig. 3a). The profile of the PersL emission spectrum is consistent with that of the steady-emission spectrum, indicating that both PersL and steady-state emission are derived from the same transitions of Bi^{3+}. Fig. 3b presents the PersL decay spectra of $LaGaO_3$:Bi after X-ray irradiation. The intensity of UV PersL initially increases and then decreases with an increase in Bi concentration. The optimal concentration is determined to be 0.1% Bi for both PersL and PL. The intensity attenuation of $LaGaO_3$:0.1%Bi within 1000 s is within an order of magnitude, and the decay curve is approximate to a straight line. It is underscored that this slow decay characteristic is extremely attractive for the acquisition of ultra-long PersL materials.

2.2 Defect and trap analysis for PersL

Detailed experimental characterization of the structure and potential defects in this system was subsequently performed. The chemical or electronic state of the elements was characterized by the X-ray photoelectron spectroscopy (XPS) measurement. As displayed in Fig. 4a, both Bi $4f_{7/2}$ and $4f_{5/2}$ core-level spectra of $LaGaO_3$:2%Bi can be deconvoluted into two peaks according to the asymmetry of shoulders and peaks. The main peak of Bi 4f at higher energy (164.1 eV, 159 eV) belongs to the Bi^{3+} in the BiO_{12} polyhedron. The pair of Bi 4f at lower energy (162.2 eV, 157.2 eV) shows the partial reduction of Bi ions. It is believed that the shoulders on the low-energy side are related to the presence of low-value Bi induced by a small number of Vo. Videlicet, it could be attributed to the strong covalency in the Bi–O band because Vo is around the Bi ions to form the oxygen-deficient $[BiO_{12-m}]$ (m < 12) units. Additionally, the content of Vo may be at a very low level because the Ga 2p peaks remain unchanged as the Bi ion concentration increases (Fig. 4b).

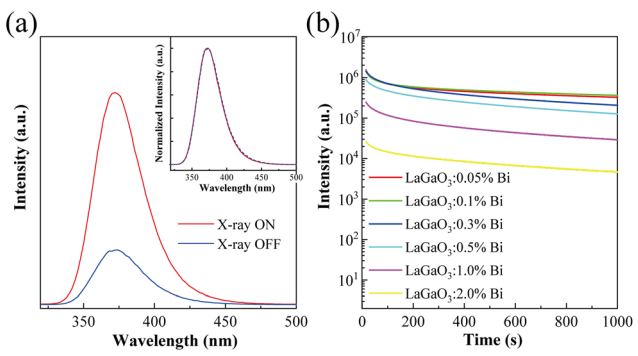

Fig. 3 (a) The emission spectra of $LaGaO_3$:0.1%Bi^{3+} recorded under X-ray radiation and after 5 min X-ray irradiation (interval 1 min). Inset: Normalized curves. (b) PersL decay curves of $LaGaO_3$:*x*Bi (*x* = 0.05–2%) measured at 15 s after irradiation by X-ray for 5 min.

The oxygen-deficient microenvironment was confirmed by Raman patterns in Fig. S1,† which exhibited an excellent match with reported Raman-active modes in the wavenumber range of 50–500 cm^{-1} for $LaGaO_3$.[28] This result suggests that the long-range structure and symmetry of the perovskite are maintained. However, $LaGaO_3$:*x*Bi of relatively high concentration (*x* = 1%, 2%) exhibits one weak band at 510 cm^{-1}. This new Raman-active band is likely to be generated from the microenvironment around Bi ions, which may be the vibration mode related to the oxygen-deficient $[BiO_{12-m}]$ units.

Considering that Vo probably plays an important role in controlling the trapping of carriers and then the PersL properties, absorption spectra measurements aimed at probing whether Vo holds the potential to function as traps required for PersL are initiated. As shown in Fig. 5a, there is a dominating band below 300 nm, which is due to the absorption of the $LaGaO_3$ host, and the background band, which extends from 250–700 nm, is probably due to defect absorption. After Bi ion doping, two peaks appear at 262 and 308 nm due to the $^1S_0 \rightarrow {}^1P_1$, $^3P_{1,0}$ optical transition of Bi^{3+} ions. Compared with the absorption curve of the $LaGaO_3$ host, when the Bi doping concentration is less than 1%, the absorption band in the range of 250–700 nm is significantly reduced, which may be due to the reduced content of Vo that usually acts as an absorption competitor in the $LaGaO_3$ host. Furthermore, the value of bandgap

Published on 21 Kudo 2024. Downloaded on 09/10/2024 2:28:35 PM.

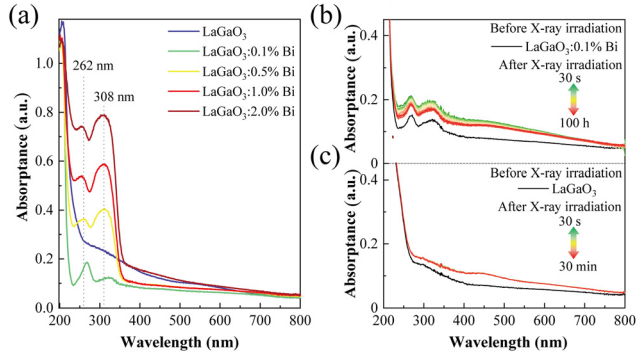

Fig. 5 (a) Absorption spectra of the Bi-doped and undoped $LaGaO_3$ samples in the initial state. Detrapping process of (b) $LaGaO_3$:0.1%Bi^{3+} and (c) the undoped $LaGaO_3$ at different times after excitation by X-ray for 5 min.

(E_g) is determined based on the Tauc plot as shown in Fig. S2.† The E_g is estimated to be about 5.8 and 5.5 eV for $LaGaO_3$:0.1%Bi and the $LaGaO_3$ host, respectively. The gap at a separation of 0.3 eV is the sub-bandgap that arises due to the formation of a donor level below the conduction band. This defect energy level in $LaGaO_3$ before Bi^{3+} doping is strongly expected to originate from the Vo. Combining the previous XPS results suggests that doping with Bi^{3+} ions will reduce the total defect content in the host at the expense of inducing Vo to approach the Bi ion sites.

The origin of PersL is studied in more detail with the *in situ* absorption spectra by examining the charge carrier trapping–detrapping process. Given the above, the absorption band from 250 nm to 700 nm is attributed to the Vo. Fig. 5b shows the variation of in-line absorption of the as-made $LaGaO_3$:0.1%Bi during the de-trapping process after the X-ray irradiation. The absorption intensity initially increases greatly, compared to the as-obtained $LaGaO_3$:0.1%Bi, and then decreases gradually after the interruption of X-ray irradiation that lasts from 30 s to 100 h. Moreover, the PersL decay curves show a similar trend in the fading of the absorption spectrum (Fig. S3†). Hence, the fading of the absorption and PersL intensity of the $LaGaO_3$:0.1%Bi sample is most likely attributed to the decrease in the trapped charge, which can be thermally released from the Vo.

As shown in Fig. 5c, a similar additional absorption band of undoped $LaGaO_3$ appears but remains unchanged over time after X-ray irradiation. After 30 minutes, the loss of the additional absorption intensity of $LaGaO_3$:0.1%Bi is about 13% (Fig. 5b, S3†) while $LaGaO_3$ is completely unchanged (Fig. 5c). Similar charging processes further prove that the trap center is an intrinsic defect (Vo) of the $LaGaO_3$ host, but the different detrapping process indicates that the UV PersL relies on the energy transfer from the trap center to the Bi^{3+} emitters. For the undoped $LaGaO_3$ host, the stored energy can only be released through lattice vibration, resulting in no PersL from the $LaGaO_3$ host after X-ray irradiation. Additionally, the additional absorption band of both undoped and Bi-doped $LaGaO_3$, after exposure to X-ray irradiation or UV light, can recover back to the original state after exposure to a red LED lighter (Fig. S4†). This finding also suggests that the trap center comes from the intrinsic defect of the material rather than the defect caused by irradiation.

The above results strongly indicate that the carriers are created and trapped at the Vo and then produce PersL by releasing the carriers or energy (produced by carrier recombination) to the nearby Bi^{3+} emitters. During the PersL process, trapped electrons or holes are thermally released individually. Therefore, it is theoretically possible to observe new EPR signals due to an odd number of holes or electrons in $LaGaO_3$:Bi after X-ray irradiation. However, the EPR spectrum shows no new signals and exhibits no fading behavior at 1 min and 10 min after X-ray irradiation (Fig. S5†). This suggests that the charges released at room temperature are actually neutral electron–hole pairs (excitons) instead of electrons or holes.

2.3 PersL improvement of $LaGaO_3$:Bi by codoping with Sb^{3+}

To further improve the PersL, different contents of Sb^{3+} are codoped into $LaGaO_3$:0.1%Bi (Fig. S6†). Compared to $LaGaO_3$:0.1%Bi, the PersL intensity of the optimal sample $LaGaO_3$:0.1%Bi,0.05%Sb integrated within 1000 s is about 2.7 times as intense as the former (inset of Fig. 6a). Fig. 6a displays the ultra-long PersL decay curves of $LaGaO_3$:0.1% Bi,0.05%Sb monitored at 372 nm under the excitation of X-ray. Data are plotted as a function of the PersL intensity (I) *versus* time (t) and the recording lasted for 100 h. The PersL of $LaGaO_3$:0.1%Bi,0.05%Sb can persist for over 2000 h (Fig. 6b and c), and after 2000 h, the emission intensity is still more than one order of magnitude stronger than the background

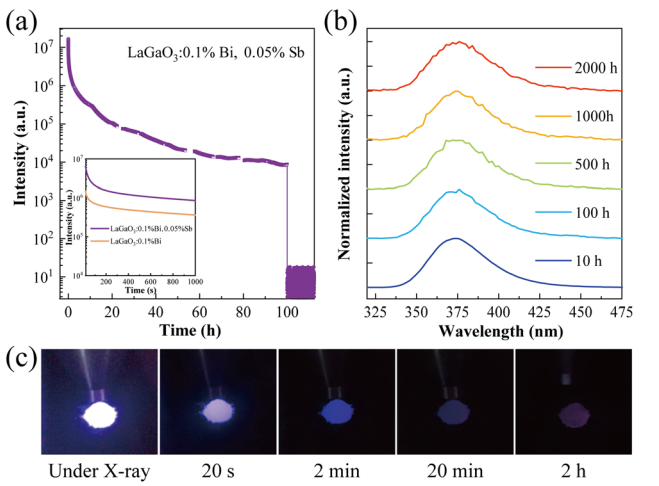

Fig. 6 (a) UV PersL decay curve of $LaGaO_3$:0.1%Bi,0.05%Sb monitored at 372 nm after 15 min of X-ray source irradiation. Note that the discrete parts of the spectra are due to the intermittent measurement artifacts. Inset: PersL decay curves of $LaGaO_3$:0.1%Bi,0.05%Sb and $LaGaO_3$:0.1% Bi. (b) The normalized persistent emission spectra of $LaGaO_3$:0.1% Bi,0.05%Sb recorded at different times after interruption of X-ray irradiation. (c) UVA images of $LaGaO_3$:0.1%Bi,0.05%Sb taken under and at different interval times (0 s to 2 h) after 5 min of X-ray irradiation.

This journal is © the Partner Organisations 2024

Published on 21 Kudo 2024. Downloaded on 09/10/2024 2:28:35 PM.

signal of the detection system. A series of UVA-PersL materials were synthesized according to the procedure described in the literature.[15,29–35] As illustrated in Fig. 7a, although the initial intensity of $LaGaO_3$:Bi,Sb is slightly weaker than that of $LiYGeO_4$:Bi, due to the extremely slow decay rate of $LaGaO_3$:Bi, Sb, the PersL intensity exceeds that of all other samples at 1000 s. After 1 h and 5 h, the intensity of $LaGaO_3$:Bi,Sb is about five times and fifteen times higher than that of $LiYGeO_4$:Bi, respectively, surpassing all other samples (Fig. 7b).

Previously, the role of Sb^{3+} ions in improving PersL performance has been discussed in detail in the case of the Cr/Sb codoped $LaGaO_3$ system.[24] Analogously, independent of the existence or nonexistence of the Sb^{3+} ions, the emission and PersL emission spectra of $LaGaO_3$:0.1%Bi are almost identical for X-ray excitation (Fig. S7,† Fig. 3a). However, Fig. S8† shows that the codoping of Sb^{3+} ions decreases the absorption intensity of the band from 250 nm to 700 nm of Bi-doped $LaGaO_3$, which may be due to the reduced content of Vo in the host. Consider the changes in the absorption fading curve and PersL decay curve occurring after codoping of Sb ions. All curves exhibit an increase in intensity and follow the same attenuation trend after X-ray irradiation (Fig. S3,† Fig. 6a). It suggests that the energy storage efficiency of traps is significantly enhanced by codoping of Sb^{3+} ions.

2.4 Thermoluminescence properties and PersL mechanism

The PersL performance is determined by two key factors: trap depth and carrier density. Based on the aforementioned discussion, the trap center in $LaGaO_3$ is the Vo. To evaluate the trap density and depth of the trapped exciton in the present case, TL spectra of Bi-doped and Bi/Sb-codoped $LaGaO_3$ samples are measured. In general, the TL intensity corresponds to the density of the trapped carriers, and it is obvious that the optimum Bi^{3+} concentration for both TL and PersL intensity was 0.1% (Fig. S9,† Fig. 3b). Besides, the TL intensity of $LaGaO_3$:0.1%Bi is increased by Sb^{3+} codoping (Fig. 8a). Similar TL features except the intensity indicate that both Bi-doped and Bi/Sb-codoped $LaGaO_3$ samples have the same defects. The incorporation of the Sb^{3+} ion may increase the density of excitons trapped at Vo, thus producing the ultra-long PersL. Furthermore, to clarify the low- and high-temperature peaks and related traps located around 350 K and 431 K, a peak-shape method was utilized to obtain the TL parameters by fitting the experimental data according to the general order kinetics formula.[36] Therefore, the calculated trap depths of doped $LaGaO_3$ were 0.78 eV and 1.12 eV (Fig. S10†), respectively. These observations demonstrate that two kinds of traps, which may originate from two kinds of Vo, participated in the PersL.

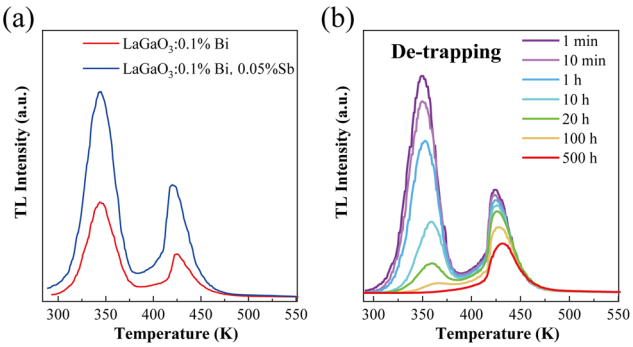

Fig. 8 (a) TL curves of $LaGaO_3$:0.1%Bi and $LaGaO_3$:0.1%Bi,0.05%Sb at 10 s after X-ray charging for 5 min. (b) TL curves of $LaGaO_3$:0.1% Bi,0.05%Sb at various decay durations after excitation by X-ray for 10 min.

Fig. 8b shows the interval time-dependent TL curves of $LaGaO_3$:0.1%Bi,0.05%Sb. With increasing interval time, no TL peak shift can be detected and only the peak intensity changed. With increasing decay time, the peak intensity of 350 K decreases sharply, and the one at 431 K decreases slightly at the same time. After 100 h of decay, the low-temperature band is weak but clear. Upon further increasing the decay time, the low-temperature band completely disappears after 500 h. As the decay time increases further, the high-temperature band will decrease gradually, and the PersL can last for 2000 h, suggesting that the emptying of both the shallow and deep traps is the effective source of the UV PersL in the whole process. Besides, as the irradiation time of X-ray light increases from 1 min to 20 min, both the peak intensities at 350 K and 431 K enhance gradually (Fig. S11†). This means that codoped $LaGaO_3$ has a huge capacity for energy storage. As we know, a shallow depth of around 0.6–0.7 eV is often stated as ideal for PersL, whereas deep traps (>1 eV) are harder to empty. In this case, PersL can be supported by the deep trap in the whole process, which means that the process of energy collection and conversion probably occurs in the vicinity of Bi^{3+} emitters by the tunneling process, inherently supporting an ultra-long UV PersL process.

The combined analyses based on the optical and structural information lead us to conclude that intrinsic Vo is the trap center. The current work shows several indications that the PersL mechanism in $LaGaO_3$:Bi involves the releasing and

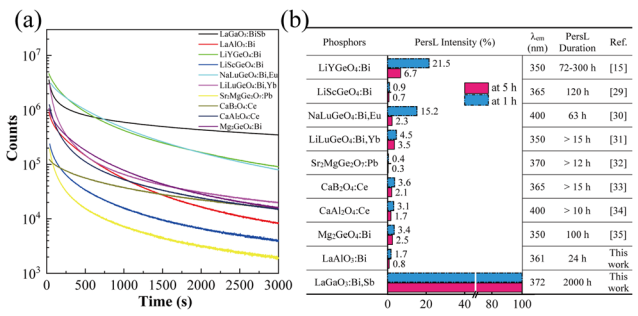

Fig. 7 (a) PersL decay curves of several ultra-long UVA PersL reported phosphors measured at 60 s after 10 min of X-ray irradiation. (b) Comparison of PersL intensity of different UVA PersL phosphors 1 h and 5 h after 10 min of X-ray excitation. The PersL intensity was normalized by $LaGaO_3$:Bi,Sb at 1 h and 5 h. Note that the PersL duration of other UVA PersL materials was extracted from references.

Published on 21 Kudo 2024. Downloaded on 09/10/2024 2:28:35 PM.

trapping of neutral electron–hole pairs, and this mechanism is localized in the vicinity of Bi ions. A plausible mechanism for the UV PersL is proposed (as schematized in Fig. 9a): (i) excitation of charge carriers: an X-ray photon being absorbed leads to the creation of an ionized, high-energy free electron. This high-energy electron then collides with atoms, especially heavy ones such as La and Bi in the host, initiating a cascade-like process that generates more ionized electrons. Lower energy collisions can also lead to the excitation of valence band electrons into the conduction band, creating numerous electron–hole pairs (process ①); (ii) storage of carriers: the created carriers are then subject to thermalization and captured by traps in the form of electron–hole pairs (process ②). Besides, after excitation, the Bi^{3+} ion returns to its $^1S_0$ ground state while the energy may also transfer to adjacent Vo to form bonds with electron–hole pairs (process ③); (iii) release and recombination of carriers: the traps are filled after a sufficient illumination period. Then, the energy is produced by recombination processes of electron–hole pairs from both shallow and deep traps, followed by transfer to the Bi^{3+} ions through the conduction band or tunneling channel (processes ④ and ⑤). Finally, the excited Bi^{3+} ion releases the energy through the $^3P_1 \rightarrow {}^1S_0$ transition (process ⑥) that causes the UV PersL. The model highlights the importance of the local electric field generated by the neighboring Vo and its local structure in facilitating carrier storage, separation, and recombination (Fig. 9b).

The above results unambiguously signify that the Vo-associated local structure served as traps involved in the PersL. More interestingly, this design idea for seeking the intrinsic oxygen-defect perovskite as a PersL host can be readily extended to the development of new PersL compounds. For instance, this design idea was transplanted into similarly structured $LaAlO_3$, which has also received considerable attention as the host of oxygen-ion conductors.[37] Experimental data indicate that Bi-doped $LaAlO_3$ exhibits excellent UV PersL, detectable for nearly 24 hours at 361 nm emission (Fig. S12†). Moreover, the oxygen-defect $LaGaO_3$ can be used as a host not only for UV PersL but also for NIR PersL by using Cr^{3+} ions as emitters, which has been described in the previous study.

2.5 $^1O_2$ generation by X-ray-excited-PDT

Motivated by the excellent UV PersL performance of $LaGaO_3$:Bi,Sb activated by low-dose X-rays, a UV PersL-mediated PDT platform ($LaGaO_3$:Bi,Sb@g-C_3N_4) was constructed by combining $LaGaO_3$:Bi,Sb particles with g-C_3N_4 (Fig. 10a). The soft polymer nature of g-C_3N_4 allows it to coat easily on the surface of $LaGaO_3$:Bi,Sb particles, forming the UV PersL-mediated PDT platform, as shown in Fig. 10b. In this integrated platform, $LaGaO_3$:Bi,Sb is a strong luminescent material that can convert X-ray to UV photons by delayed conversion in real-time. Meanwhile, there exists a substantial overlap between the X-ray-activated PersL of $LaGaO_3$:Bi,Sb and the absorption spectrum of g-C_3N_4 (Fig. 10c). Thus, it is hypothesized that when the $LaGaO_3$:Bi,Sb@g-C_3N_4 composite is irradiated by X-ray, $LaGaO_3$:Bi,Sb can relay energy as UV photons to g-C_3N_4 and thus produce cytotoxic $^1O_2$.

To investigate this effect, a common singlet oxygen ($^1O_2$) indicator, DPBF, was employed, which is a commercially available probe for detecting $^1O_2$ generation in cells or solutions by measuring the decrease in fluorescence (ex/em: 410/455 nm). Impressively, we monitored $^1O_2$ generation with a $LaGaO_3$:Bi,Sb@g-C_3N_4 composite solution (4 mg mL^{-1}) after X-ray irradiation (0.51 Gy). The intensity of 455 nm fluorescence was decreased by 15% at 15 min after X-ray irradiation (Fig. 10d). Comparable experiments were conducted using acetonitrile solutions, $LaGaO_3$:Bi,Sb particles, and g-C_3N_4, all of which show a smaller decrease (<3%) of fluorescence at 15 min (Fig. 10e). These data indicate that $^1O_2$ can be efficiently produced when all three components—g-C_3N_4, $LaGaO_3$:Bi,Sb, and X-ray—are present, supporting that $^1O_2$ production is a result of UV PersL-mediated energy transfer. Moreover, in the PDT experiments with the $LaGaO_3$:Bi,Sb@g-C_3N_4 composite, the X-ray irradiation dose (0.51 Gy) is notably lower than the doses commonly used in clinical radiotherapy (5 Gy).[38]

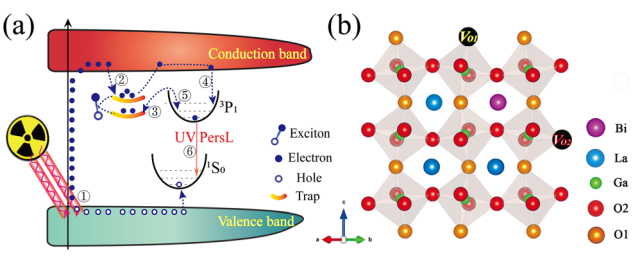

Fig. 9 (a) Proposed PersL mechanism of $LaGaO_3$:Bi,Sb. The arrows represent electron transfer processes and optical transitions. (b) Schematic diagram of Bi and two kinds of neighbor Vo (black ball) in the $LaGaO_3$ structure.

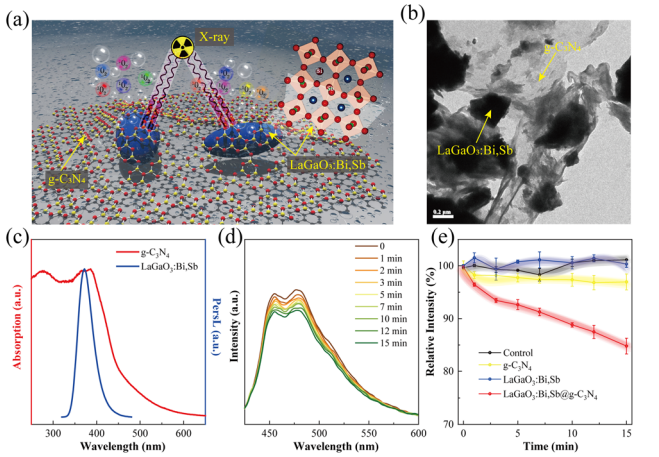

Fig. 10 (a) Schematic representation of the X-ray-activated PDT mechanism based on $LaGaO_3$:Bi,Sb@g-C_3N_4. (b) TEM image of $LaGaO_3$:Bi,Sb@g-C_3N_4 particles. (c) Effective overlap between the absorption of g-C_3N_4 and the PersL of $LaGaO_3$:Bi,Sb. (d) Photoluminescence intensity changes in DPBF-containing solutions of $LaGaO_3$:Bi,Sb@g-C_3N_4 after X-ray irradiation. (e) Comparison of $^1O_2$ production using DPBF as an indicator (ex/em: 410/455 nm).

This journal is © the Partner Organisations 2024

Published on 21 Kudo 2024. Downloaded on 09/10/2024 2:28:35 PM.

3. Conclusions

According to the requirements of some potential applications based on UV PersL, a new UV-emitting PersL material Bi-doped $LaGaO_3$ has been successfully demonstrated by understanding the origin of the trap center. Systemic characterization led us to conclude that the intrinsic Vo in the $LaGaO_3$ host stores energy and acts as the trap center. Under X-ray excitation, Sb co-doped $LaGaO_3$:Bi features a UV PersL peaking at 372 nm with an ultra-long PersL exceeding 2000 h. Leveraging these unique attributes, the proposed PDT platform showcased remarkable efficiency in *in vitro* applications, even with low-dose X-ray irradiation (0.51 Gy). This breakthrough not only surpassed the traditional depth barrier for tissue penetration, but also resulted in a substantial reduction in X-ray dosage. Thus, it is widely acknowledged that the X-ray-activated UV PersL material holds immense promise for light-mediated therapies in deep tissue and beyond.

4. Experimental section

4.1 Materials and synthesis

Ga_2O_3 (99.99%), La_2O_3 (99.99%), Bi_2O_3 (99.99%), and Sb_2O_3 (99.99%), purchased from Aladdin Reagent Co., Ltd, were selected as raw materials. The polycrystalline $La_{1-x}GaO_3$:xBi (x = 0–5%) was synthesized by a solid-state reaction. Stoichiometric amounts of La_2O_3, Ga_2O_3, and Bi_2O_3 powder were mixed and ground thoroughly in an agate mortar with ethanol. The mixtures were then heated at 1000 °C for 2 h and were re-sintered at 1300 °C for 5 h. After cooling to RT and re-grinding again, the final products were obtained for measurements. For the synthesis of $La_{1-x}Bi_xGa_{1-y}O_3$:Sb_y,Bi_x (x = 0.1–2%; y = 0.03–1%), La_2O_3, Ga_2O_3, Bi_2O_3, and Sb_2O_3 powders were used, while other synthesis parameters are the same with the Bi single doped sample.

4.2 g-C_3N_4-modified $LaGaO_3$:Bi,Sb

g-C_3N_4 was synthesized by heating guanidine hydrochloride to 600 °C for 3 h in air. The typical preparation of the $LaGaO_3$:Bi, Sb@g-C_3N_4 platform is as follows: a specific amount of g-C_3N_4 was mixed with methanol and sonicated for 10 h to ensure complete dispersion. Finely ground $LaGaO_3$:0.1%Bi,0.05%Sb powder was then added to the solution mentioned above and stirred for 24 h. The powder was obtained after drying at 100 °C for 24 h. Finally, the $LaGaO_3$:Bi,Sb@g-C_3N_4 platform with a weight ratio of 4% g-C_3N_4 was successfully synthesized.

4.3 Detection of singlet oxygen

DPBF (1,3-diphenylisobenzofuran, Sigma, 99%) served as a probe for detecting $^1O_2$. Specifically, the $LaGaO_3$:Bi,Sb@g-C_3N_4 composite (4 mg mL^{-1}) was mixed with DPBF (5 μM, 200 μL) and then exposed to an X-ray light source (0.51 Gy min^{-1}) for 1 min. DPBF rapidly reacts with $^1O_2$, allowing the estimation of $^1O_2$ production by measuring the luminescence intensity of DPBF.

4.4 Charging of persistent phosphors

The product underwent irradiation using a mini-X X-ray tube (Amptek, Inc.) with a fixed setting at 50 kV and 79 μA for all experiments conducted. The radiation dose is calibrated by using a ^{137}Cs radiation unit (0.546 mGy min^{-1}) and Thermoluminescence Dosemeters circular chips LiF:Mg,Ti.

4.5 Characterization

X-ray diffraction (XRD) for phase identification was conducted using a diffractometer (Rigaku D/MAX 2200 VPC), operating at 40 kV and 26 mA with Cu Kα radiation (λ = 1.5405 Å). The Raman spectra were captured employing a Raman microscope system (Renishaw inVia) with a 514.5 nm laser as the excitation source. All samples were evaluated in three separate locations and exhibited similar Raman spectra. X-ray photoelectron spectroscopy (XPS) spectra were obtained using an X-ray photoelectron spectrometer (Thermo Fisher Scientific ESCALAB 250) equipped with monochromatic Al Kα radiation (E = 1486.2 eV). Diffuse absorbance spectra were obtined by using a Varian Cary 5000 UV–vis spectrophotometer. Room-temperature photoluminescence (PL), photoluminescence excitation (PLE), and persistent luminescence (PersL) spectra and decay curves were obtained using a spectrofluorometer (Edinburgh Instruments FLS1000) equipped with a 500 W xenon lamp. The electron paramagnetic resonance (EPR) spectra were recorded using an EPR spectrometer (Bruker model A300). The thermoluminescence (TL) curves were collected with a TL spectrophotometer (Guangzhou Radiation Technology LTTL-3DS). The samples underwent X-ray irradiation for 5 min before TL measurement and were subsequently measured with a linear heating rate of 1 K s^{-1} within the temperature range of 300–600 K. The size and morphology of the samples were observed on a transmission electron microscope (TEM, FEI Tecnai G2 F30) operated at 300 kV.

Author contributions

H. Z. and J. W. designed the research; B.-M. L. performed the experiments; B.-M. L., Y. Lin, and Y. Liu analyzed the data and wrote the paper; B.-M. L., S. Zhang, J. Zhu, H. Z., and J. W. revised the paper.

Conflicts of interest

The authors declare no conflicts of interest at the time of submission.

Acknowledgements

The authors are grateful to the Foshan Science and Technology Bureau (Foshan Science and Technology Innovation Project, 1920001000150-08), the National Natural Science Foundation of China (52102195), the Joint Funds of the National Natural

Published on 21 Kudo 2024. Downloaded on 09/10/2024 2:28:35 PM.

Science Foundation of China and Yunnan Province (U1902222), the Guangdong Provincial Science & Technology Project (2022A0505050032) and the Major Science and Technology Research and Development Project of Jiangxi Province (20223AAE01003) for the financial support.

References

1 L. Liang, J. Chen, K. Shao, X. Qin, Z. Pan and X. Liu, Controlling persistent luminescence in nanocrystalline phosphors, *Nat. Mater.*, 2023, **22**, 289–304.
2 K. Huang, N. Le, J. S. Wang, L. Huang, L. Zeng, W. C. Xu, Z. Li, Y. Li and G. Han, Designing Next Generation of Persistent Luminescence: Recent Advances in Uniform Persistent Luminescence Nanoparticles, *Adv. Mater.*, 2022, **34**, 2107962.
3 J. Yang, Y. Liu, Y. Zhao, Z. Gong, M. Zhang, D. Yan, H. Zhu, C. Liu, C. Xu and H. Zhang, Ratiometric Afterglow Nanothermometer for Simultaneous in Situ Bioimaging and Local Tissue Temperature Sensing, *Chem. Mater.*, 2017, **29**, 8119–8131.
4 G. Cui, X. Yang, Y. Zhang, Y. Fan, P. Chen, H. Cui, Y. Liu, X. Shi, Q. Shang and B. Tang, Round-the-Clock Photocatalytic Hydrogen Production with High Efficiency by a Long-Afterglow Material, *Angew. Chem., Int. Ed.*, 2019, **58**, 1340–1344.
5 T. Matsuzawa, A New Long Phosphorescent Phosphor with High Brightness, $SrAl_2O_4$:Eu^{2+}, *J. Electrochem. Soc.*, 1996, **143**, 2670.
6 X. Wang, Z. Zhang, Z. Tang and Y. Lin, Characterization and properties of a red and orange Y_2O_2S-based long afterglow phosphor, *Mater. Chem. Phys.*, 2003, **80**, 1–5.
7 H. Yamamoto and T. Matsuzawa, Mechanism of long phosphorescence of $SrAl_2O_4$:Eu^{2+},Dy^{3+} and $CaAl_2O_4$:Eu^{2+},Nd^{3+}, *J. Lumin.*, 1997, **72**, 287–289.
8 D. Jia, L. A. Lewis and X.-j. Wang, Cr^{3+}-Doped Lanthanum Gallogermanate Phosphors with Long Persistent IR Emission, *Electrochem. Solid-State Lett.*, 2010, **13**, J32.
9 Z. Pan, Y. Y. Lu and F. Liu, Sunlight-activated long-persistent luminescence in the near-infrared from Cr^{3+}-doped zinc gallogermanates, *Nat. Mater.*, 2011, **11**, 58–63.
10 S. Zhang, J. Xiahou, X. Sun and Q. Zhu, Incorporation of Mg^{2+}/Si^{4+} in $ZnGa_2O_4$:Cr^{3+} to Generate Remarkably Improved Near-Infrared Persistent Luminescence, *Coatings*, 2022, **12**, 1239.
11 C. Wang, F. Liu, H. Wu, L. Zhang, J. Zhang, X.-j. Wang and Y. Liu, Extended Excitation Approach for Ultraviolet Phosphors via the White-to-Ultraviolet Upconversion, *J. Phys. Chem. C*, 2023, **127**, 18213–18218.
12 X. Zhao, F. Liu, Z. Yu, X. Li, C. Wang, F. Chen and X.-j. Wang, Sunlight stimulated solar-blind ultraviolet phosphor, *Phys. Rev. Res.*, 2022, **4**, L012028.
13 S. Yan, F. Liu, J. Zhang, X.-j. Wang and Y. Liu, Persistent Emission of Narrowband Ultraviolet-B Light upon Blue-Light Illumination, *Phys. Rev. Appl.*, 2020, **13**, 044051.
14 Y. M. Yang, Z. Y. Li, J. Y. Zhang, Y. Lu, S. Q. Guo, Q. Zhao, X. Wang, Z. J. Yong, H. Li, J. P. Ma, Y. Kuroiwa, C. Moriyoshi, L. L. Hu, L. Y. Zhang, L. R. Zheng and H. T. Sun, X-ray-activated long persistent phosphors featuring strong UVC afterglow emissions, *Light: Sci. Appl.*, 2018, **7**, 88.
15 J. Shi, X. Sun, S. Zheng, X. Fu, Y. Yang, J. Wang and H. Zhang, Super-Long Persistent Luminescence in the Ultraviolet A Region from a Bi^{3+}-Doped $LiYGeO_4$ Phosphor, *Adv. Opt. Mater.*, 2019, **7**, 1900526.
16 L. Liu, J. Xu, Y. Li, S. Peng, P. Lin, H. Zhong, L. Song, J. Shi, X. Sun and Y. Zhang, Developing dual-mode material with ultraviolet and visible persistent luminescence for multi-mode anti-counterfeiting and information encryption, *Inorg. Chem. Front.*, 2023, **10**, 3131–3138.
17 X. Wang and Y. Mao, Emerging Ultraviolet Persistent Luminescent Materials, *Adv. Opt. Mater.*, 2022, **10**, 2201466.
18 X. Wang and Y. Mao, Recent advances in Pr^{3+}-activated persistent phosphors, *J. Mater. Chem. C*, 2022, **10**, 3626–3646.
19 W. Sun, Z. Zhou, G. Pratx, X. Chen and H. Chen, Nanoscintillator-Mediated X-Ray Induced Photodynamic Therapy for Deep-Seated Tumors: From Concept to Biomedical Applications, *Theranostics*, 2020, **10**, 1296–1318.
20 J. Zhou, K. An, P. He, J. Yang, C. Zhou, Y. Luo, W. Kang, W. Hu, P. Feng, M. Zhou and X. Tang, Solution-Processed Lead-Free Perovskite Nanocrystal Scintillators for High-Resolution X-Ray CT Imaging, *Adv. Opt. Mater.*, 2021, **9**, 2002144.
21 L. Song, P.-P. Li, W. Yang, X.-H. Lin, H. Liang, X.-F. Chen, G. Liu, J. Li and H.-H. Yang, Low-Dose X-ray Activation of W(VI)-Doped Persistent Luminescence Nanoparticles for Deep-Tissue Photodynamic Therapy, *Adv. Funct. Mater.*, 2018, **28**, 1707496.
22 H. Suo, X. Zhang and F. Wang, Controlling X-ray-activated persistent luminescence for emerging applications, *Trends Chem.*, 2022, **4**, 726–738.
23 L. Feng, F. He, B. Liu, G. Yang, S. Gai, P. Yang, C. Li, Y. Dai, R. Lv and J. Lin, G-C_3N_4 Coated Upconversion Nanoparticles for 808 nm Near-Infrared Light Triggered Phototherapy and Multiple Imaging, *Chem. Mater.*, 2016, **28**, 7935–7946.
24 B. M. Liu, R. Zou, S. Q. Lou, Y. F. Gao, L. Ma, K. L. Wong and J. Wang, Low-dose X-ray-stimulated $LaGaO_3$:Sb,Cr near-infrared persistent luminescence nanoparticles for deep-tissue and renewable in vivo bioimaging, *Chem. Eng. J.*, 2021, **404**, 127133.
25 Y. Katayama, H. Kobayashi and S. Tanabe, Deep-red persistent luminescence in Cr^{3+}-doped $LaAlO_3$ perovskite phosphor for in vivo imaging, *Appl. Phys. Express*, 2014, **8**, 012102.
26 Y. Tang, M. Deng, M. Wang, X. Liu, Z. Zhou, J. Wang and Q. Liu, Bismuth-Activated Persistent Phosphors, *Adv. Opt. Mater.*, 2022, **11**, 2201827.
27 R. Floresperez, D. Zemlyanov and A. Ivanisevic, Quantitative evaluation of covalently bound molecules on GaP (100) surfaces, *J. Phys. Chem. C*, 2008, **112**, 2147–2155.

 This journal is © the Partner Organisations 2024

Published on 21 Kudo 2024. Downloaded on 09/10/2024 2:28:35 PM.

28 T. Inagaki, Raman studies of $LaGaO_3$ and doped $LaGaO_3$, *Solid State Ionics*, 1999, **118**, 265–269.
29 Y. Zhang, D. Chen, W. Wang, S. Yan, J. Liu and Y. Liang, Long-lasting ultraviolet-A persistent luminescence and photostimulated persistent luminescence in Bi^{3+}-doped $LiScGeO_4$ phosphor, *Inorg. Chem. Front.*, 2020, **7**, 3063–3071.
30 W. Wang, Z. Sun, X. He, Y. Wei, Z. Zou, J. Zhang, Z. Wang, Z. Zhang and Y. Wang, How to design ultraviolet emitting persistent materials for potential multifunctional applications: A living example of a $NaLuGeO_4$:Bi^{3+},Eu^{3+} phosphor, *J. Mater. Chem. C*, 2017, **5**, 4310–4318.
31 H. Cai, Z. Song and Q. Liu, Infrared-photostimulable and long-persistent ultraviolet-emitting phosphor $LiLuGeO_4$:Bi^{3+},Yb^{3+} for biophotonic applications, *Mater. Chem. Front.*, 2021, **5**, 1468–1476.
32 Y. Liang, F. Liu, Y. Chen, K. Sun and Z. Pan, Long persistent luminescence in the ultraviolet in Pb^{2+}-doped $Sr_2MgGe_2O_7$ persistent phosphor, *Dalton Trans.*, 2016, **45**, 1322–1326.
33 S. K. Sharma, M. Bettinelli, I. Carrasco, J. Beyer, R. Gloaguen and J. Heitmann, Dynamics of Charges in Superlong Blacklight-Emitting CaB_2O_4:Ce^{3+} Persistent Phosphor, *J. Phys. Chem. C*, 2019, **123**, 14639–14646.
34 D. Jia and W. M. Yen, Trapping Mechanism Associated with Electron Delocalization and Tunneling of $CaAl_2O_4$:Ce^{3+}, A Persistent Phosphor, *J. Electrochem. Soc.*, 2003, **150**, H61.
35 C. Wang, Y. Jin, J. Zhang, X. Li, H. Wu, R. Zhang, Q. Yao and Y. Hu, Linear charging-discharging of an ultralong UVA persistent phosphor for advanced optical data storage and wide-wavelength-range detector, *Chem. Eng. J.*, 2023, **453**, 139558.
36 A. J. J. Bos, Theory of thermoluminescence, *Radiat. Meas.*, 2006, **41**, S45–S56.
37 M. Islam, M. Cherry and L. Winch, Defect chemistry of $LaBO_3$ (B = Al, Mn or Co) perovskite-type oxides. Relevance to catalytic and transport behaviour, *J. Chem. Soc., Faraday Trans.*, 1996, **92**, 479–482.
38 H. Chen, G. D. Wang, Y. J. Chuang, Z. Zhen, X. Chen, P. Biddinger, Z. Hao, F. Liu, B. Shen, Z. Pan and J. Xie, Nanoscintillator-mediated X-ray inducible photodynamic therapy for in vivo cancer treatment, *Nano Lett.*, 2015, **15**, 2249–2256.